A Novel Approach for Simulating Atmospheric Optical Turbulence Seeing Parameters

Randall J. Alliss

Northrop Grumman Corporation
7575 Colshire Drive
Mclean, VA 22102

Abstract

Quantifying atmospheric seeing for applications such as LADAR, spaced based imaging, and optical communications is not new. Much effort and expense has been expended to develop ground-based instrumentation to estimate optical turbulence so that mitigation techniques can be developed. Instruments, such as a Differential Imaging Motion Monitors (DIMM), which track stars or solar DIMMs which track the sun are often deployed to collect measurements. These field collection campaigns require many years of observations which are costly but essential to develop mitigation techniques. Adaptive optics (AO) systems are a common form of ground-based turbulence mitigation, particularly for space domain awareness and coherent space to ground optical communications, but they are often custom and very expensive. Because of the complexity and high costs, it is critical to avoid over engineering the AO system based on observations that can take many years to collect. As ground-based optical ground stations begin to proliferate the ability to quickly model and estimate atmospheric seeing is critical and is now possible given the availability and low cost of high-performance computing.

The severity of optical turbulence can be characterized by the refractive index structure function C_n^2, which in turn is used to calculate atmospheric seeing parameters through various integration equations. While attempts have been made to characterize C_n^2 using empirical models (e.g., Huffnagel-Valley), a novel method for computing C_n^2 has been developed. Using an atmospheric Numerical Weather Model (NWM), the index of refraction is more directly computed using three dimensional modeled pressure, temperature, thermal stability, vertical wind shear, turbulent Prandtl number, and turbulence kinetic energy (TKE). NWMs are three dimensional models of the atmosphere that include full physics, dynamics, and thermodynamics, by solving the Navier-Stokes equations numerically. These models have been greatly improved over the years and are enhanced by advances in numerical data assimilation particularly from meteorological satellites. In this work, we use an advanced NWM customized to generate high resolution vertical profiles of C_n^2 from the surface layer to the top of the atmosphere allowing for both horizontal, slantwise and vertical seeing estimates of the Fried Coherence length (r_o), Greenwood frequency ($\mathcal{F}_g$) and Isoplanatic angle (Θ_o). Simulations, which take just a few weeks to run on a modest high-performance computing system, are capable of producing multiple years of realistic seeing parameters.

The custom NWM model is configured to run at 1 kilometer (km) horizontal resolution over a 60 km by 60 km region. The resolution of the vertical levels is approximately 60-m below 3 km above ground level (AGL), 70-200 m between 3–12 km AGL, and 200-500 m up to the model top (10 millibars). The Mellor-Yamada-Janjic (MYJ) TKE scheme is modified to diagnose the turbulent Prandtl number as a function of the Richardson number, following observations by Kondo and others. This modification deweights the contribution of the buoyancy term in the equation for TKE by reducing the ratio of the eddy diffusivity of heat to momentum. This is necessary particularly in the stably stratified free atmosphere where turbulence occurs in thin layers not typically resolvable by these kinds of models. The modified MYJ scheme increases the probability and strength of TKE in thermally stable conditions thereby increasing the probability of optical turbulence. Over two years of simulations have been generated for several desert locations, one in each hemisphere. Results indicate realistic values of the seeing parameters and model output matches the expected diurnal variations for one of the desert sites. As expected, seeing is worse during the daytime summer (2 cm r_o) than at night with large r_o's observed just after sunset and just before sunrise during the atmospheric neutral event.

This paper will review the NWM and the necessary modifications required for accurate seeing parameter estimations. Results from several desert locations, thought to have the most challenging optical turbulence for an AO system, will be shown including the seasonal and diurnal variations evident in the data.

1. Introduction

With High Performance Computing (HPC) platforms becoming much more affordable and accessible, simulations of physical parameters in the atmosphere are more easily performed. An excellent example of this is free space optical turbulence (OT). OT is an important atmospheric phenomenon, particularly for astronomers, because of the impact it has on seeing. Small-scale temperature and moisture fluctuations in the atmosphere result in fluctuations of the refractive index. The wave front of radiation traveling through the atmosphere changes as it encounters inhomogeneities in the refractive index, degrading optical image quality. The intensity of the turbulent fluctuations of the atmospheric refractive index is described by the refractive index structure function, C_n^2. The ability to quantify the amount of OT above an observatory and to understand its vertical distribution is vital and can impact decisions on adaptive optics design, observatory scheduling, and site selection for new observatories. Although instruments have been developed to characterize OT, they are expensive to maintain over long durations of time and the quality is limited.

Numerical simulations of OT are an attractive alternative to local observations in regions where infrastructure (i.e., electrical power) is lacking. Numerical simulations offer many advantages over direct measurements. These advantages include a three-dimensional description of C_n^2 over regions of interest, simulations that can be performed anywhere on earth at any time, and the ability to provide forecasts of OT that could be used for observational scheduling purposes. The reliability of these types of simulations for describing the climatology of OT has recently been shown to be quite good.

Our approach to simulate OT employs a model used to predict tropospheric weather. These models are referred to by the meteorological community as Numerical Weather Models (NWM). NWM are routinely used by meteorologists to predict everyday weather. However, in this application the model is modified to make simulations of C_n^2. In this paper we describe how NWM is leveraged to simulate OT and present various results for two locations.

2. Technical Approach

In this study we use version 3.9.1 of the Weather Research and Forecasting (WRF) model developed jointly by the National Center for Atmospheric Research (NCAR) and the National Oceanic and Atmospheric Administration (NOAA) [1]. WRF is a mesoscale NWM model developed for the prediction of weather and is routinely used by the National Weather Service and other forecasting services. The model is based on the Navier Stokes equations, which are solved numerically on a three-dimensional grid. Four basic atmospheric properties are simulated by the model from which all others variables are derived. These properties are wind, pressure, temperature, and atmospheric water vapor.

This study used the WRF model to develop a climatology of OT over several desert locations. Some of the benefits of this novel approach include the ability to model turbulence at sites with no in situ measurements, ability to produce a climatology of seeing parameters, ability to identify vertical structure of the atmosphere (e.g. temperature inversions, local wind maxima, etc.) and to identify orographic influences, and to investigate r_0 as a function of year, month and time of day. The following sections describe the model setup, modifications to the code, and derivation of OT parameters followed by results of simulations performed to date.

a. Model Setup

WRF is used to simulate daily meteorological conditions for several desert locations in the Northern and Southern Hemisphere for the years 2019 and 2020. The model is configured at 1-km horizontal resolution with dimensions of 60x60 grid points and 144 vertical levels. The resolution of the vertical levels is approximately 60-m below 3 km above ground level (AGL), 70-200 m between 3–12 km AGL, and 200-500 m up to the model top (10 millibars). Simulations are initialized at 1200 UTC directly from the 36-km Global Forecasting System (GFS) analysis produced by the National Weather Service. Lateral boundary conditions are provided out to 36 hours by three-hourly GFS forecasts. This allows for filtering out model "spin-up" by excluding the first three simulation hours, while still capturing the full 24-hour diurnal cycle. Selected physics and diffusion options are summarized in Table 1.The model was reinitialized each day during the two year period.

Table 1. Physics and diffusion settings used in WRF model for this study

Time Integration	RK3
Time Step	2 sec
Horizontal/Vertical Advection	Fifth/Third order
Explicit Diffusion	Physical space 2D deformation, no sixth order
Boundary Layer Physics	Mellor, Yamada, Janjic (MYJ)
Surface Layer	Janjic Eta
Land Surface	Noah
Shortwave/Longwave Radiation	Dudhia/RRTM
Microphysics	WSM6
Cumulus Parameterization	None

b. Model Modifications

The minimum turbulence kinetic energy (TKE) permitted in the Mellor-Yamada-Janjic (MYJ) scheme had to be modified. The default setting gives TKE values > 0.1 m^{2}s^{-2}, resulting in unrealistically large values of C_n^2 in the free atmosphere. Following Gerrity et.al. (1994) [2], the minimum TKE limit was changed to 10^{-5} m^{2}s^{-2}. The second modification involves the eddy diffusivities of heat and momentum (K_H and K_M, respectively). In the original MYJ scheme, these variables are given by

$$K_h = l_q S_H \quad , K_h = l_q S_M,$$

Where l is the mixing length, $q = \sqrt{2TKE}$, and S_H, and S_M, are functions of TKE, mixing length, buoyancy, and vertical wind shear (Mellor and Yamada, 1982)[3]. In the modified version these relationships are unchanged for neutral and unstable conditions. However, when the gradient Richardson number (Ri) > 0.01, an implementation by Walters and Miller, 1994 [4] is followed whereby K_M is adjusted according to:

$$\frac{K_H}{K_M} = \begin{cases} \dfrac{1}{7Ri,} & for Ri \geq 1, \\[2em] \dfrac{1}{6.873Ri + \dfrac{1}{1+6.873Ri}} & for 0.01 < Ri \leq 1. \end{cases}$$

The $\dfrac{K_H}{K_M}$ equation was first proposed by Kondo et.al. (1978) [5]. The Kondo equation decreases $\dfrac{K_H}{K_M}$ with increasing

Ri, effectively increasing the TKE production by vertical wind shear. This is necessary to generate free atmospheric turbulence that is commonly associated with jet streams. Without this change the model rarely produces TKE larger than the model's minimum value, something that is considered unrealistic when compared to many global thermosonde measurements.

c. Derivation of Seeing

This study is interested in the vertical distribution of the refractive index structure function C_n^2. When turbulence is locally homogeneous and isotropic, C_n^2 is related to changes in the refractive index. Large values of C_n^2 correspond to increasing changes in the refractive index and thus greater turbulence. Tatarskii, 1971 [6] derived an alternative expression for the structure function parameter applicable for optical wavelengths:

$$C_n^2 = \left(\frac{79 * 10^{-8} P}{T^2} \right)^2 C_T^2$$

where P is atmospheric pressure, T is air temperature, and C_T^2 is the structure function parameter for temperature. C_T^2 is given by:

$$C_T^2 = a^2 \left(\frac{K_H}{K_M} \right) L_o^{\frac{4}{3}} \left(\frac{\partial \theta}{\partial Z} \right)^2$$

Where a^2 is an empirical constant, L_o is the outer length scale of turbulence (i.e., the upper bound of the inertial subrange), and $\left(\frac{\partial \theta}{\partial Z} \right)$ is the vertical gradient of potential temperature. Following Walters and Miller, a^2 is set to 2.8 and calculation of the outer length scale of turbulence in the thermally stable conditions is approximated from Deardorff, 1980 [7]:

$$L_o = 0.76 \sqrt{\frac{TKE}{N}}$$

where N is the Brunt-Vaisala frequency. In thermally unstable conditions, L_o is related to the depth of the unstable boundary layer.

In this study we also compute Fried's Coherence Length (r_o), which is a measure of phase distortion of an optical wave front by turbulence. r_o can vary rapidly over time and from one point of the sky to another. This parameter represents the integrated effect of turbulence along a line of sight. Larger (smaller) values of r_o are indicative of less (more) turbulence and better seeing. After Fried, 1965 [8], it is calculated by integrating C_n^2 along a path, z:

$$r_o = \left[0.423 \left(\frac{2 \Pi}{\lambda} \right)^2 \int_0^\infty C_n^2(z) dz \right]^{-3/5}$$

4

3. Results

Three-dimensional turbulence simulations were made over several desert locations including both Northern and Southern Hemisphere regions between 2019 and 2020. Figure 1 shows the distribution of r_0 for 2019 and 2020 over a Southern Hemisphere desert location. The results are broken down by day (0800 – 1600 local time), night (2000 – 0500 local time) and all hours. All values are referenced to 500 nanometers (nm) and zenith. As expected, the median r_0 during the day (2.9 cm) is lower than at night (3.5 cm), signaling large turbulence due to day time heating.
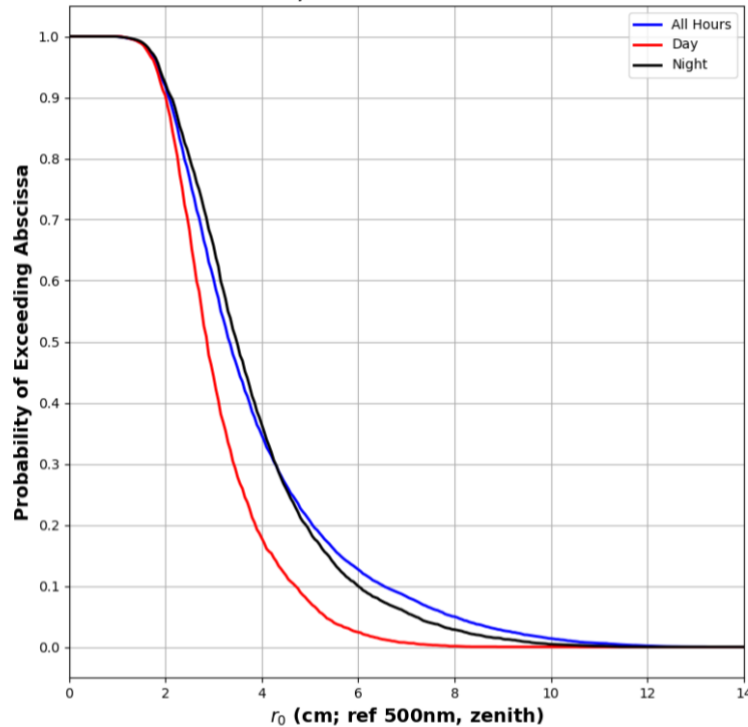

Figure 1. Distribution of r_0 over a Southern Hemisphere desert location.

Figure 2 shows the distribution of r_0 as a function of time of year. Figure (a,b,c,d) shows spring, summer, fall, and winter respectively. Spring consists of September, October, November, Summer consists of December, January, February, Fall consists of March, April, May and Winter consists of June, July and August. Values of r_0 are lowest during the daytime when surface heating is greatest, except for winter months when the worst seeing is typically at night.

The diurnal variability of r_0 is given is figure 3. Figure 3 shows the median, 5th and 95th percentile values of r_0 for each hour of the day for times when there is cloud free line of sight to zenith. As expected, the smallest values of r_0 occur during midday, during the strongest solar heating with median r_0's around 2.2 cm. Significant variations however are seen in the 5th and 95th percentiles. A large evening neutral event around 1800 is also seen in the simulations. R_0 more than doubles during the evening neutral event with values as high as 8 cm. The evening neutral event occurs when a decoupling of the boundary layer and free atmosphere occurs resulting in significantly stable atmospheric conditions. At night the expected increase of r_0 is not observed in the simulations which is atypical for a good astronomical site. Much investigation was performed to determine why the simulations do not show the nighttime minimum (i.e., large r_0) in optical turbulence. Results indicate the presence of a persistent low level nocturnal jet due to significant wind shear which increases turbulence just above the planetary boundary layer. Figure 4 shows an

5

example of a low level nocturnal jet as simulated by the model. A West to East cross section of the horizontal wind through the model domain is shown. The y-axis shows the height above the ground. Bright colors (red and yellow) indicate where the winds are strongest several km above the surface. This persistent low level jet at nighttime is responsible for the relatively poor seeing conditions observed in the statistics. However, this low level jet is most commonly found during the site's winter months of June, July and August.
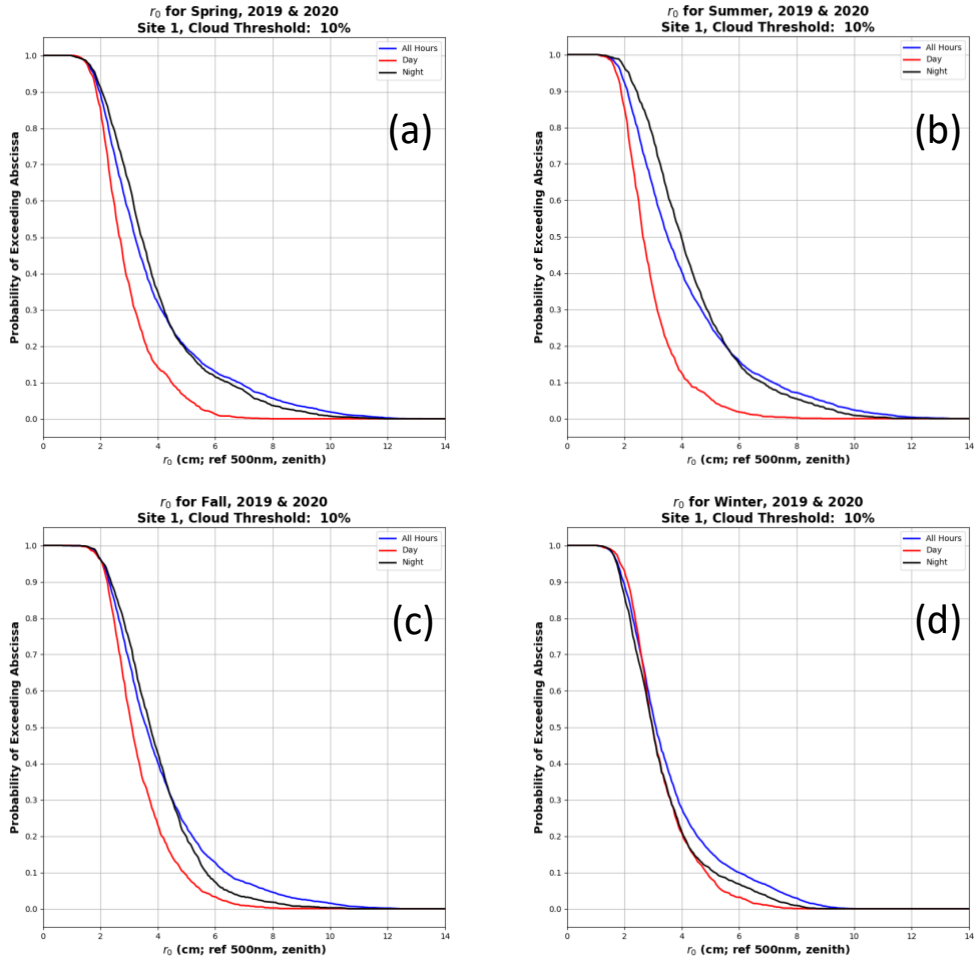
Figure 2. Distribution of r_0 as a function of season. (a) Spring, (b) Summer, (c) Fall, (d) Winter. Median values of r_0 are lowest during the daytime except during winter months.
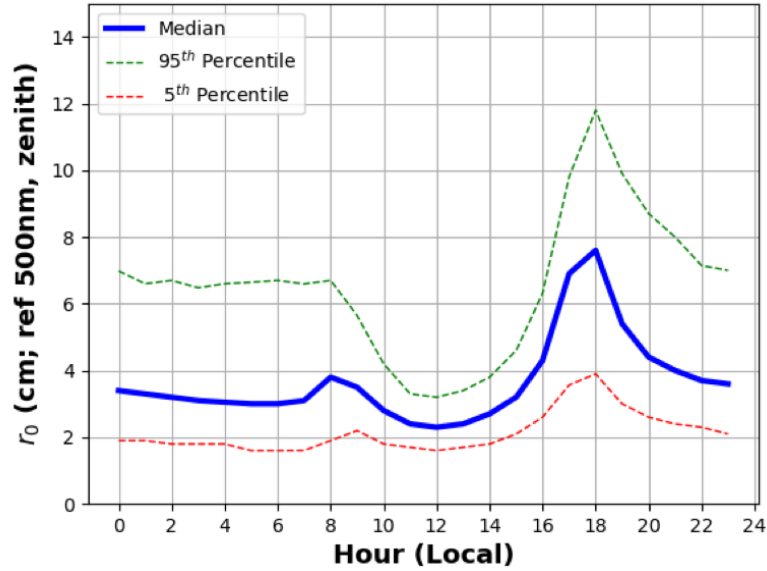
6

Figure 3. The diurnal variation of r_0 with the 5th and 95th percentiles also shown. All values are referenced to 500 nm and to zenith. Values of r_0 are suppressed at night due to a persistent low level jet.
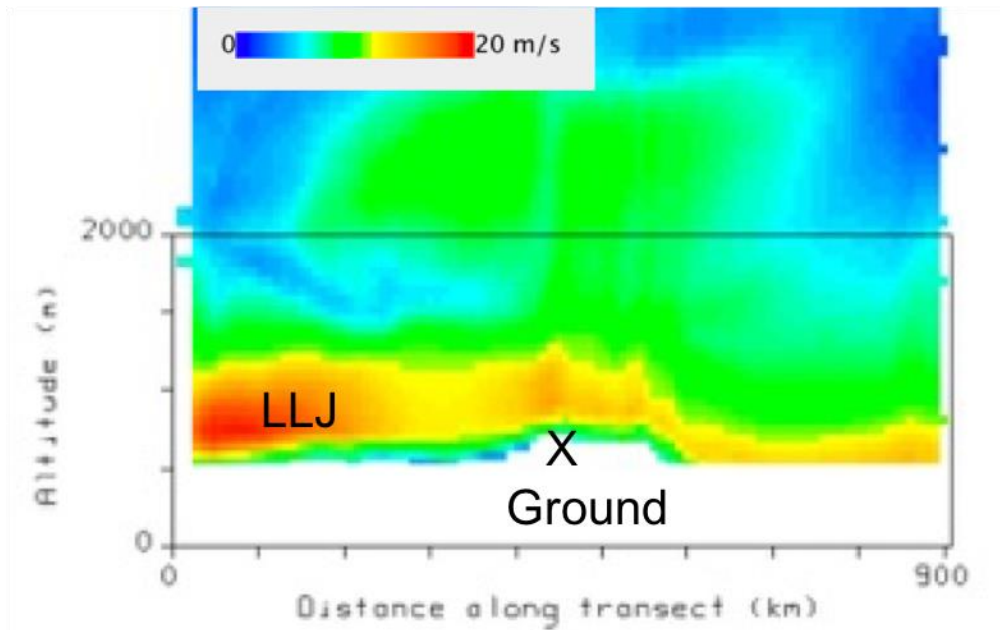

Figure 4. Vertical cross section of the horizontal wind along a West to East transect through the model domain. Bright colors (red and yellow) indicate where winds are strongest. X marks the location of the seeing parameter analysis.

A Northern Hemispheric site near the Mediterranean Sea was also simulated for a two year period. Figure 5 shows the cumulative distribution of r_0 for all daytime (0800 – 1600 local time, red), nighttime (2000 - 0500 local time, black) and all cases.
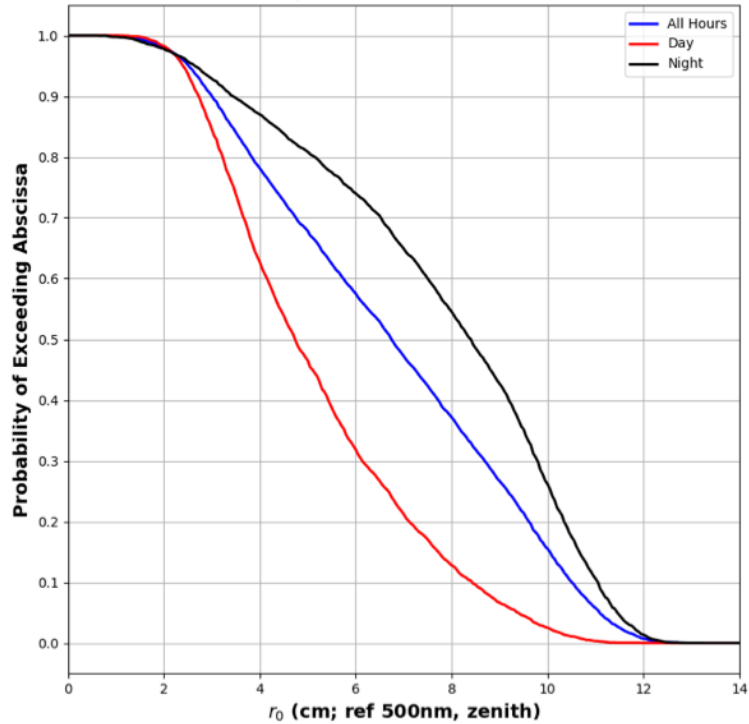

Figure 5. Distribution of r_0 over a Nothern Hemisphere location during day, night and all times. Median values of r_0 are higher compared to the Southern hemisphere site.

Values of r_0 are referenced to 500 nm and zenith. The values of r_0 are dramatically different than the Southern hemisphere site. A median r_0 value of 4.7 cm is simulated during the daytime and 8.4 cm at night. This is much more consistent with good astronomical seeing. Overall the median r_0 for all times is greater than 6.8 cm. Despite the sites relatively arid environment its proximity to the sea and its stabilizing effects on the atmosphere are the main contributor to the excellent seeing conditions.

Figure 6 shows how the seeing changes as a function of time of year. Spring consists of March, April, May Summer consists of June, July and August, Fall consists of September, October, November, and Winter consists of December, January, February. Values of r_0 are lowest during the daytime when surface heating is greatest even during the winter months (d). During summer the simulations produce median r_0 of slightly less than 4 cm. Winter months produce the most similar day night values of r_0 as is typically expected.
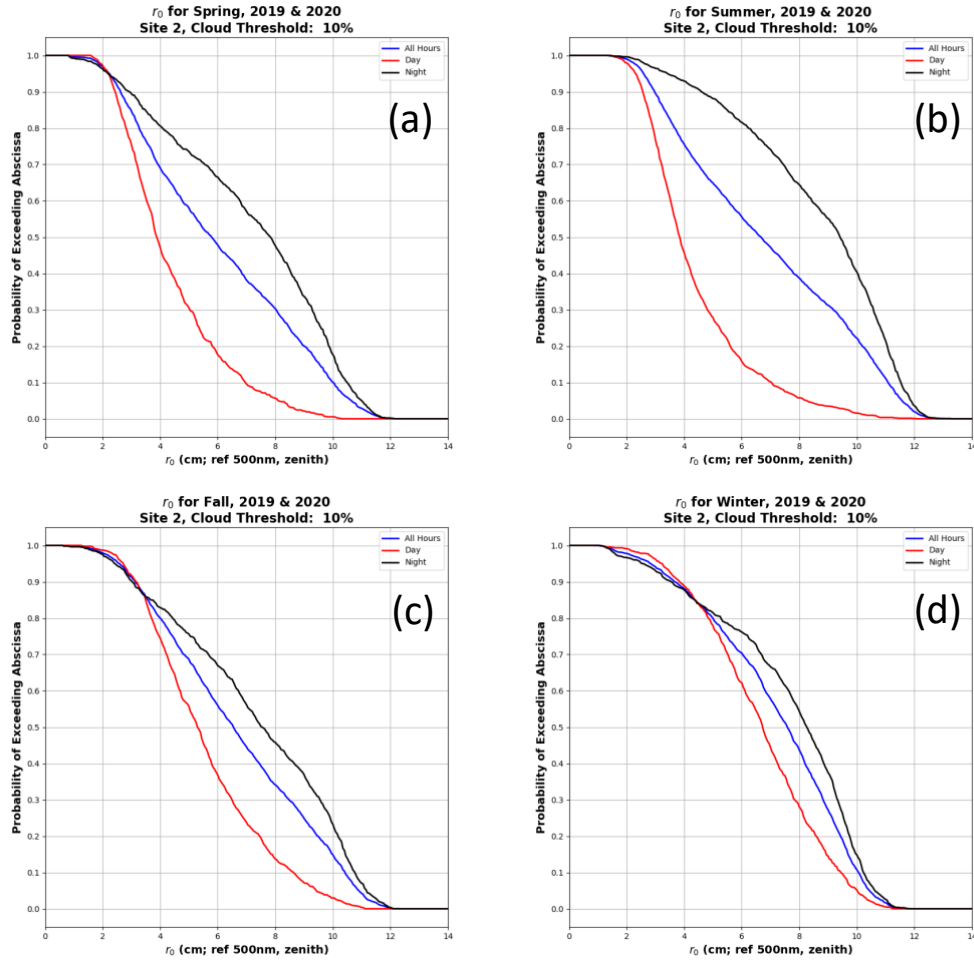
Figure 6. Distribution of r_0 as a function of season. (a) Spring, (b) Summer, (c) Fall, (d) Winter. Median values of r_0 are lowest during the daytime spring and summer and largest at night.

Figure 7 shows the median diurnal variation of r_0. The 5th and 95th percentile of r_0 are also shown. Unlike the Southern Hemisphere site, the diurnal variation of the Northern Hemisphere site shows a much more classic variation with maximum r_0 during night and minimum during the daytime. There is only a small indication of an evening neutral event at this site. The difference between nighttime and daytime r_0's is nearly 4 cm.
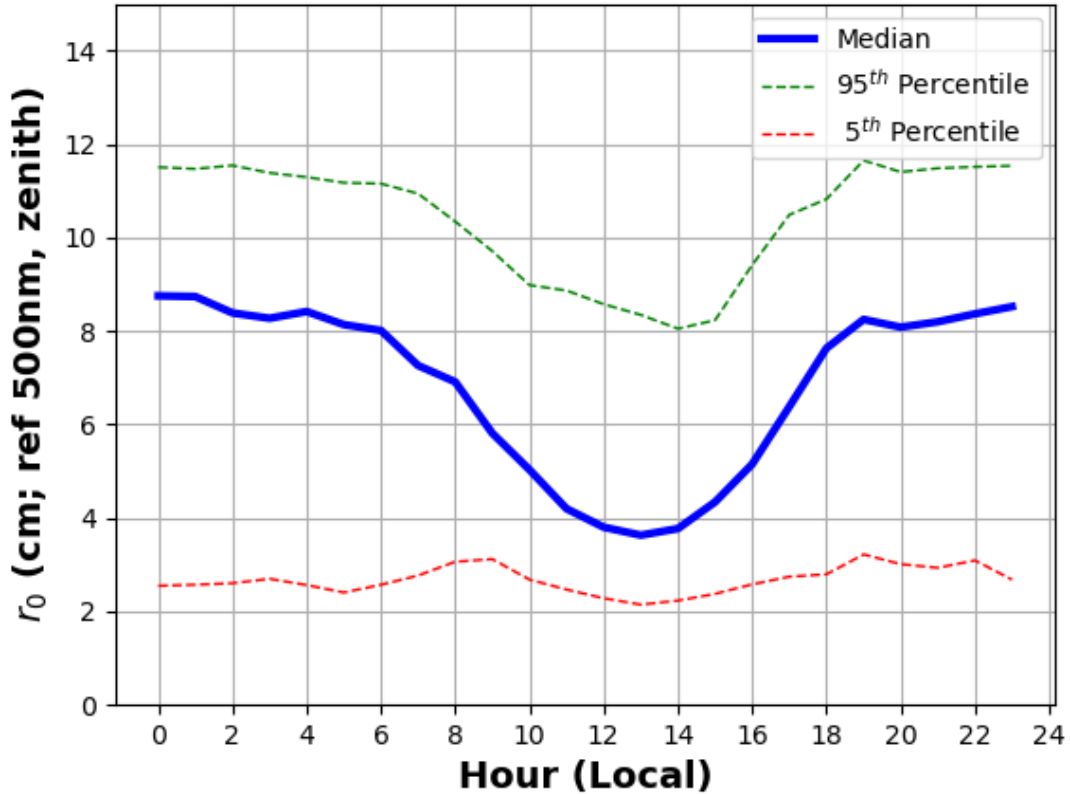
9

Figure 7. The diurnal variation of r_0 with the 5th and 95th percentiles also shown. All values are referenced to 500 nm and to zenith. A classic nighttime maximum and daytime minimum in r_0 is apparent.

Figure 8 shows the diurnal variation of r_0 as a function of season. Spring consists of March, April, May Summer consists of June, July and August, Fall consists of September, October, November, and Winter consists of December, January, February. All seasons show the classic diurnal variation of minimum r_0 during the day and maximum at night with the winter months showing the least amount of variation. The 5th percentile r_0 never gets below 2 cm regardless of time of day or season. As expected, the diurnal variation is largest during the spring and summer months.
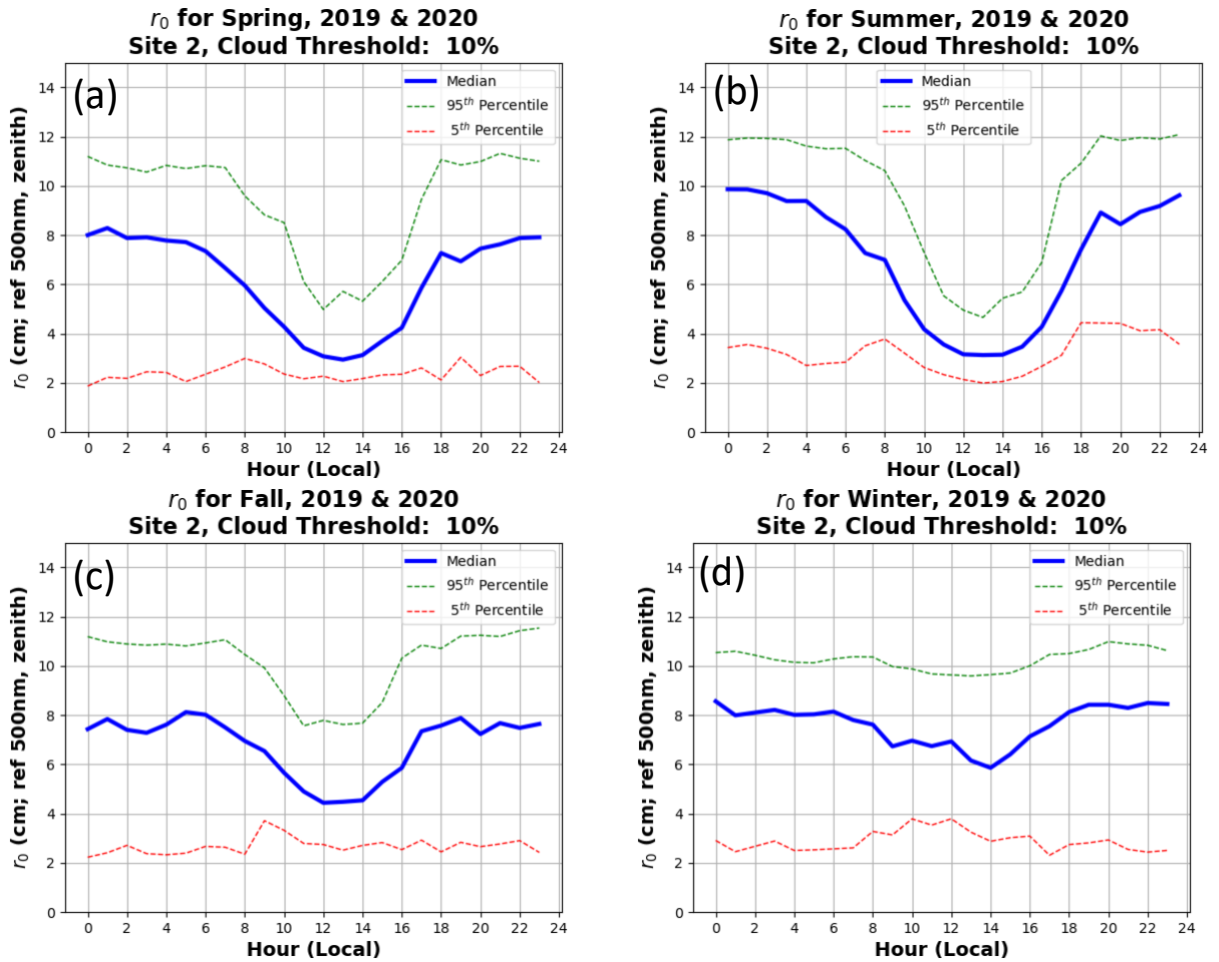
Figure 8. Diurnal variation in r₀ as a function of season. (a) Spring, (b) Summer, (c) Fall, (d) Winter. The diurnal variation in ro is very apparent during Spring, Summer and Fall and less somewhat suppressed in the winter. The 5ᵗʰ percentile always exceed 2 cm.

For comparison, both sites climatology of the Fried Coherence Length are shown in Table 2 below. Overall, the Northern Hemisphere site has twice the value of r_0 as the Southern Hemisphere site. Daytime median values at the Southern Hemisphere site during its summer are as low as 2.6 cm and while they are on the order of 3.8 cm at the Northern Hemisphere site.

Table 2. Comparison in Fried Coherence Length between the Southern and Northern Hemisphere sites.

Median Values of r_0 (cm). Values are referenced to 500 nm and zenith

		All Data	Spring	Summer	Fall	Winter
Southern Hemisphere	Day	2.9	2.7	2.6	3.1	3.0
	Night	3.5	3.4	4.0	3.7	3.0
	All Hours	3.3	3.2	3.5	3.6	3.1

		All Data	Spring	Summer	Fall	Winter
Northern Hemisphere	Day	4.7	3.9	3.8	5.3	6.7
	Night	8.4	7.8	9.4	7.5	8.3
	All Hours	6.7	5.8	6.7	6.6	7.6

4. Summary and Next Steps

A novel approach using a numerical weather model (NWM) to simulate optical turbulence seeing parameters has been developed and applied to two desert locations. Simulations of optical turbulence are performed for a two year period. Although the NWM is incapable of simulating the very smallest values of r_o, it is capable of generally describing the climatology of the site of interest. This makes the model very convenient to use over areas where observations are not possible or are limited. The model does an excellent job simulating the diurnal variation found in turbulence. Site two shows the typical diurnal variation in seeing while the desert site in the Southern Hemisphere showed an atypical distribution. This was caused by a persistent wintertime nocturnal low level jet which increased turbulence during these times. Efforts to compare these simulations to in situ measurements are underway. These simulations of optical turbulence are being used by designers of optical communication systems and for overall system risk reduction studies. An effort to simulate the seeing parameters in realtime for situational awareness is also underway.

References

[1] Skamarock, W. C., J. B. Klemp, J. Dudhia, D. O. Gill, D. M. Barker, M. G. Duda, X.-Y. Huang, W. Wang, and J. G. Powers, 2008: A description of the advanced research WRF version 3. NCAR Technical Note, NCAR/TN-475+STR, 113 pp.

[2] Gerrity, J. P., T. L. Black, and R. E. Treadon, 1994: The numerical solution of the Mellor-Yamada level 2.5 turbulent kinetic energy equation in the Eta model. *Mon. Wea. Rev.*, **122**, 1640–1646.

[3] Mellor, G. L., and T. Yamada, 1982: Development of a turbulence closure model for geophysical fluid problems. *Rev. Geophys. Space Phys.*, **20**, 851–875.

[4] Walters, D. L., and D. K. Miller, 1999: Evolution of an upper-tropospheric turbulence event—comparison of observations to numerical simulations. *Preprints, 13th Symposium on Boundary Layer Turbulence*, AMS, 157–160, Dallas, TX.

[5] Kondo, J., O. Kanechika, and N. Yasuda, 1978: Heat and momentum transfers under strong stability in the atmospheric surface layer. *J. Atmos. Sci.*, **35**, 1012–1021.

[6] Tatarskii, V. I., 1971: The effects of the turbulent atmosphere on wave propagation. Technical Report, U.S. Department of Commerce, NTIS TT-68-50464, 472 pp.

[7] Deardorff, J. W., 1980: Stratocumulus-capped mixed layers derived from a three-dimensional model. *Bound.-Layer Meteor.*, **18**, 495–527.

[8] Fried, D. L., 1965: Statistics of a geometric representation of wavefront distortion. *J. Opt. Soc. Amer.*, **55**, 1427–1435.